Recent shift from dominant nitrogen to CO_2 fertilization control on the growth of mature Qinghai spruce in a wet and cold Qilian Mountains forest

Ziyi Wang [a], Xiaohong Liu [a, *], Josep Peñuelas [b, c], J. Julio Camarero [d], Xiaomin Zeng [a], Xueyan Liu [e], Liangju Zhao [f, *], Guobao Xu [f, g], Lixin Wang [h]

[a] *School of Geography and Tourism, Shaanxi Normal University, Xi'an 710119, China*

[b] *National Research Council of Spain (CSIC), Global Ecology Unit CREAF-CSIC-UAB, Bellaterra, Catalonia 08193, Spain*

[c] *CREAF, Cerdanyola del Valles, Catalonia 08193, Spain*

[d] *Instituto Pirenaico de Ecología (IPE-CSIC), Zaragoza 50080, Spain*

[e] *School of Earth System Science, Tianjin University, Tianjin 300072, China*

[f] *Shaanxi Key Laboratory of Earth Surface System and Environmental Carrying Capacity, College of Urban and Environmental Sciences, Northwest University, Xi'an 710069, China*

[g] *State Key Laboratory of Cryospheric Science, Northwest Institute of Eco-Environment and Resources, Chinese Academy of Sciences, Lanzhou 730000, China*

[h] *Department of Earth Sciences, Indiana University-Purdue University Indianapolis (IUPUI), Indiana 46202, USA*

List of Author's ORCID:

Ziyi Wang, https://orcid.org/0000-0001-7109-7119

Xiaohong Liu, https://orcid.org/0000-0002-1497-6122

Josep Peñuelas, https://orcid.org/0000-0002-7215-0150

J. Julio Camarero, https://orcid.org/0000-0003-2436-2922

Xiaomin Zeng, https://orcid.org/0000-0002-3674-228X

Xueyan Liu, https://orcid.org/0000-0003-1097-1516

Liangju Zhao, https://orcid.org/0000-0001-7445-3916

Guobao Xu, https://orcid.org/0000-0001-7267-554X

Lixin Wang, https://orcid.org/0000-0003-0968-1247

*** Corresponding authors:**

Xiaohong Liu, School of Geography and Tourism, Shaanxi Normal University, Xi'an 710119, China.

E-mail address: xhliu@snnu.edu.cn

Liangju Zhao, Shaanxi Key Laboratory of Earth Surface System and Environmental Carrying Capacity, College of Urban and Environmental Sciences, Northwest University, Xi'an 710069, China.

E-mail address: zhlj@nwu.edu.cn

Abstract

Terrestrial vegetation growth is stimulated by rising atmospheric CO_2 concentration, a warmer climate, and increased soil nutrient availability. However, as plants age, progressive nutrient limitation is known to occur, especially in mature forests where soil nitrogen is deficient. Yet the long-term growth response of mature trees to rising CO_2 accompanied by changing climate and nitrogen availability in semi-arid mountain regions is unclear. Here we used tree-ring widths and stable carbon ($\delta^{13}C$) and nitrogen ($\delta^{15}N$) isotopes to investigate the drivers of radial growth of mature Qinghai spruce (*Picea crassifolia*) in the central Qilian Mountains, northwest China, from 1840 through 2019. Tree growth benefited from improved nitrogen availability, chiefly via changes in bioavailable nitrogen pools modified by a favorable climate during 1930–1964. Enhanced intrinsic water-use efficiency (iWUE), driven by reduced stomatal conductance (g_s) related to intensive water stress, lead to radial growth declines in 1985–2002. Recent acceleration of tree growth was largely attributed to a CO_2 fertilization effect through enhanced iWUE during 2003–2019. Nitrogen availability was positively related to tree growth from the 1920s onward until greater CO_2 fertilization ensued from 2000 onward. Hence, the negative effects of low nitrogen availability on growth could be mitigated or reversed by a high atmospheric CO_2 concentration and warmer climate conditions. Our results suggest that mature spruce forests still harbor potential to increase ecosystem-level carbon sequestration and thereby partially mitigate climate warming. Such a nature-based solution in drought-prone forests would be achieved under warmer-wetter climate conditions in northwest

China.

Keywords: Stable carbon and nitrogen isotopes, Carbon sequestration, CO_2 fertilization, Spruce forests, Tree growth

1. Introduction

The climate of northwest China has been changing since the 1980s, shifting from warm-dry to warm-wet conditions, thus enhancing terrestrial vegetation productivity and forest growth (Shi et al., 2003; Wang et al., 2020). There is mounting interest in unveiling the underlying causal mechanisms by which tree growth is increased in temperate, seasonally dry forests due to changes in either atmospheric composition—increases in the ambient CO_2 concentration (c_a) and nitrogen deposition or climate (Cienciala et al., 2018; Gao et al., 2018; Mathias and Thomas, 2018; Quadri et al., 2021; Silva et al., 2016). Controlled experiments do indicate that increases in c_a can stimulate the productivity of plants and improve their resource use efficiency, thus augmenting vegetation carbon storage (Fernández-Martínez et al., 2017). However, such CO_2 fertilization effect on tree growth has not been widely confirmed under field conditions where growth is also constrained by water shortage and soil nutrients deficit (Camarero et al., 2015; Jiao et al., 2021; Norby et al., 2010; Terrer et al., 2019).

How climate change affects tree ecophysiology and forest tree growth differs under varied environmental conditions. The responses of mountain forests to higher temperatures are likely to be positive (Hember et al., 2019; Silva et al., 2016), whereas severe droughts associated with rapid global warming decrease productivity and trigger widespread tree mortality (Liang et al., 2016; Yan et al., 2021). Further, sustained anthropogenic nitrogen deposition and increased nitrogen input to soils may also promote forest productivity (Cienciala et al., 2018; Hember et al., 2019). Yet, soil nitrogen availability has fallen in some natural forest ecosystems (Craine et al., 2018;

Kou et al., 2020), with decreasing foliar nitrogen concentrations in central and southern Europe reported (Peñuelas et al., 2020). Far-reaching consequences of declines in nitrogen availability include a weakened response of trees to elevated c_a and a reduced ability of forests to sequester carbon (Mason et al., 2022; Norby et al., 2010; Terrer et al., 2019). However, determining to what extent key environmental variables impact tree growth still faces several challenges, impairing the reliability of predicting future forest carbon sink.

Forest ecosystems have already taken up a considerable portion of anthropogenic CO_2 emissions (Friedlingstein et al., 2022). Accordingly, it is imperative to assess whether mature forests will continue to function as carbon sinks as global warming intensifies (Grassi et al., 2017). Theoretically, mature trees may be less responsive than young trees to rising c_a because of increased age-related hydraulic, photosynthetic, and nutrient limitations (Jiang et al., 2020; Luo et al., 2004). Mature trees and forest stands are not expected to serve as strong carbon sinks because of the proximal equilibrium between carbon uptake and respiration (Jiang et al., 2020). However, old-growth forests still accumulate huge amounts of carbon in their woody pools because their complex stand structure that determines the capacity of forests uptake and store carbon (Stephenson et al., 2014). Additionally, for an old tree, its overall carbon sink potential might be higher than previously thought given the faster increase in tree growth rates in recent decades (Palandrani et al., 2021). Faced with these conflicting observations, the capacity of mature forests to continually sequester carbon needs to be quantified, particularly in drought-prone mountainous regions that are vulnerable to drying

conditions under future warming.

Together, tree-ring basal area increment (BAI), intrinsic water-use efficiency (iWUE) estimated from tree-ring stable carbon isotopes ($\delta^{13}C$), and stable nitrogen isotopes ($\delta^{15}N$) can be used to track and infer historical changes in forest productivity, plant physiology, and nitrogen demand relative to soil availability (McLauchlan et al., 2017; Rayback et al., 2020). Tree-ring $\delta^{13}C$ can provide insight into gas-exchange regulation and photosynthesis processes and reveal long-term tree water-use responses. As derived from the $\delta^{13}C$ values in tree rings, iWUE is a function of the carbon assimilation rate (A) and stomatal conductance (g_s) (Ehleringer et al., 1993). A greater iWUE has been linked to water limitation and an ecophysiological response of trees to increasing c_a (Saurer et al., 2004). Increases in iWUE may sometimes lead to higher rates of tree growth (Guerrieri et al., 2019; Palandrani et al., 2021; Rayback et al., 2020), but this is not always the case when interacts with other limiting abiotic factors, such as drought stress and low nutrients availability such as nitrogen (Giguere-Croteau et al., 2019; González de Andrés et al., 2021; Wang, McDowell et al., 2020). Moreover, tree-ring $\delta^{15}N$ signatures can be used to uncover long-term changes in the availability, status, and cycling of nitrogen in forest ecosystems (Gerhart and McLauchlan, 2014; Mason et al., 2022). Hence, investigating long-term trends in forest growth dynamics based on multiple tree-ring proxies holds great promise.

In this study, we used dendrochronological measurements and tree-ring isotopic proxies ($\delta^{13}C$ and $\delta^{15}N$) to examine how atmospheric CO_2, nitrogen availability, and climate variables influenced the growth patterns of mature Qinghai spruce trees in the

interior of central Qilian Mountains in China. Our aims were: (1) to analyze the growth dynamics of mature trees; and (2) to elucidate the environmental drivers of tree growth using climatic information as well as isotope-derived physiological information (i.e., iWUE and $\delta^{15}N$).

2. Material and methods

2.1. Study site and climate data

We conducted field research at the Sidalong Forest Farm (99° 54′ 10″ E, 38° 26′ 58″ N), in the central Qilian Mountains, northwest China (Fig. S1a). This study site is located on a wet and shaded slope where the dominant tree species, Qinghai spruce (*P. crassifolia*), is largely distributed at an elevation of 2600–3300 m a.s.l. The climate here is influenced by the East Asian monsoon and the Westerlies (Li and Liu, 2000). Climate records (1958–2019) from the two nearest meteorological stations (Qilian, 100° 10′ 48″ E, 38° 06′ 36″ N, 2787 m a.s.l.; Minle, 100° 29′ 24″ E, 38° 16′ 12″ N, 2271 m a.s.l.) show that the mean annual temperature is 1.0 – 4.1 °C, with total annual precipitation of 288.2 – 526.6 mm. The maximum monthly vapor pressure deficit (VPD) occurs in June while the highest monthly relative humidity (RH) is recorded in August (Fig. S1b). From 1958 to 2019, there were upward trends in mean annual temperature, total precipitation, and VPD, but a downward trend in RH (Fig. S1c).

The following monthly climate variables were obtained and used by averaging reliable data during 1958–2019 taken from both Qilian and Minle meteorological stations (China Meteorological Data Service Center, http://data.cma.cn): mean temperature, total precipitation, VPD, and RH. To calculate each VPD value, maximum

156 temperature and minimum RH were used (Guerrieri et al., 2020). Because of short
157 duration of recording in local climatic data, we extracted a gridded monthly dataset
158 (spatial resolution: 0.5°×0.5°) for mean temperature, total precipitation, VPD, and self-
159 calibrating Palmer Drought Severity Index (scPDSI) for 1935–2019 from CRU TS 4.04
160 datasets (Harris et al., 2020). Monthly VPD from this gridded data was calculated as
161 the difference between the saturation vapor pressure (estimated from temperature) and
162 vapor pressure. For the series of climate factors obtained from meteorological data and
163 CRU dataset, we assessed their temporal trends using linear regressions (Figs. S1c and
164 S2) and compared their variability through standardized Z-scores using 1958–2019 as
165 the referenced period (Fig. S3).

166 ***2.2. Field sampling and tree-ring chronology establishment***

167 At the field site, 22 mature and apparently healthy Qinghai spruce trees growing in
168 a pure natural forest stand, at an elevation of 2590 m a.s.l. were randomly selected and
169 sampled in June 2020. For each tree, its diameter at breast height (DBH) was measured
170 with a girth tape. From each tree, we extracted two 10-mm-diameter increment cores in
171 opposite directions at breast height (1.3 m above the ground), for a total of 44 obtained
172 cores.

173 All wood increment cores were air-dried and sanded using progressively finer
174 sandpapers (from 120 to 1200 grit sizes) (Stokes and Smiley, 1996). We then visually
175 cross-dated the samples by recognizing the characteristics of narrow or wide rings.
176 Tree-ring widths were measured using LINTAB 6 (RINNTECH, Heidelberg, Germany)
177 at a resolution of 0.001 mm and their cross-dating was checked by TSAP-Win and

COFECHA software (Holmes, 1983). We also employed a negative exponential function to remove the underlying biological growth trends from the raw ring-width series. To create a standardized tree-ring width chronology, we utilized the biweight robust mean to average all the individual indices in the ARSTAN program (Cook, 1985) (Fig. S4). The reliable standardized chronology, with a subsample signal strength greater than 0.85, started in 1830. We selected the period from 1840 to 2019 for analysis, excluding the initial 10 years in stable carbon and nitrogen isotope analysis to avoid potential juvenile effects.

The raw ring-width chronologies were converted into basal area increment (BAI) series, to provide a more accurate measure of changed stem woody biomass (Peters et al., 2015). BAI was calculated assuming concentric growth, as follows:

$$BAI = \pi \times (R_t^2 - R_{t-1}^2) \quad (1)$$

where R corresponds to the stem radius at year t, which is the year of ring formation (Biondi and Qeadan, 2008). If a sample lacked the pith, we estimated the missing inner diameter by applying a geometric method (Duncan, 1989), and then summed all previous ring widths to determine the tree radius at each year. The individual BAI series of all sampled trees were then averaged for the 1840–2019 period, to generate the stand-level tree growth chronology (Fig. 1a) via biweight robust means and using the 'dplR' package (Bunn et al., 2022) for R v4.1.3.

2.3. Stable isotope measurements

Five cores (one per tree) were chosen to measure both the $\delta^{13}C$ and $\delta^{15}N$ in wood and to obtain carbon-to-nitrogen ratios (C/N). All cores were cross-dated, correlated

well with the master BAI chronology (r = 0.71–0.88, $p < 0.05$), and included the 1840–2019 period. Using a stainless-steel blade, the cores were manually dissected into annual rings under a microscope; individual whole rings were then pooled into a single sample for the same year. These pooled samples were ground in a ball mill into a homogeneous fine powder (about 200-mesh) and then oven-dried at 55 °C for 48 h.

To measure the $\delta^{13}C$, $\delta^{15}N$, as well as carbon and nitrogen concentrations of the samples, we used a flash combustion method at the Laboratory of Stable Isotope and Global Change in Shaanxi Normal University (Xi'an, China). Each sample (0.07–0.08 mg for carbon and 7 mg for nitrogen isotope determination) was loaded into a tin capsule and combusted in an elemental analyzer (EA Isolink, Thermo Fisher, Bremen, Germany) interfaced with continuous flow mode to a gas isotope ratio mass spectrometer (Delta V Advantage, Thermo Fisher, Bremen, Germany). The stable isotope values are reported in delta (δ) notation (in per mil, ‰) relative to the international reference standards:

$$\delta^{13}C \text{ or } \delta^{15}N = \left(\frac{R_{sample}}{R_{standard}} - 1\right) \times 1000 \quad (2)$$

where R_{sample} and $R_{standard}$ is the ratio of ^{13}C:^{12}C or ^{15}N:^{14}N in the sample and corresponding standard, using Vienna Pee Dee Belemnite (V-PDB) and atmospheric N_2 for carbon and nitrogen isotopes, respectively. The analytical precision of the stable isotope measurements was calibrated using laboratory standard materials, Sigma-Aldrich α-cellulose ($\delta^{13}C = -24.25$ ‰), and wood internal standard from Qilian juniper (average $\delta^{15}N = -5.24$ ‰). The analytical errors (standard deviations) were 0.03 ‰ (n = 30) for $\delta^{13}C$ and 0.12 ‰ (n = 84) for $\delta^{15}N$, based on replicate measurements of the

reference standards. Further details about the quantification of $\delta^{15}N$ in tree rings can be found in Wang et al. (2022).

2.4. Calculating intrinsic water-use efficiency (iWUE)

The iWUE and ratio of leaf intercellular CO_2 to atmospheric CO_2 concentrations (c_i/c_a) were derived from the discrimination against ^{13}C ($\Delta^{13}C$). The $\Delta^{13}C$ was calculated from the tree-ring $\delta^{13}C$ as follows (Farquhar et al., 1982):

$$\Delta^{13}C = (\delta^{13}C_a - \delta^{13}C_p)/(1 + \delta^{13}C_p/1000) \quad (3)$$

where $\delta^{13}C_a$ is the isotope value of atmospheric CO_2 and $\delta^{13}C_p$ is that of tree-ring wood. The $\Delta^{13}C$ was also calculated as the following formulas:

$$\Delta^{13}C = a + (b - a) \times (c_i/c_a) \quad (4)$$

where c_a refers to atmospheric CO_2 concentration; a (~4.4 ‰) is the fractionation arising from the diffusion of CO_2 in air via stomata, and; b (~27 ‰) is the discrimination of ribulose bisphosphate against $^{13}CO_2$ during carboxylation (O'Leary, 1981). The estimated annual values of c_a and $\delta^{13}CO_2$ were obtained from the work of Belmecheri and Lavergne (Belmecheri and Lavergne, 2020). The iWUE, i.e., the ratio of assimilated carbon (A) to water loss through transpiration (stomatal conductance; g_s), was calculated as follows (Ehleringer et al., 1993):

$$iWUE = A/g_s = (c_a - c_i)/1.6 = c_a \times (1 - c_i/c_a)/1.6 \quad (5)$$

where A is the flux of net assimilation, measured as CO_2 uptake; g_s is the leaf stomatal conductance of water vapor (i.e., transpiration), and; the 1.6 value is the diffusivity ratio of water vapor relative to CO_2.Then we compared the measured iWUE series to three scenarios–constant c_i, constant c_i/c_a, and constant c_a-c_i (Fig. 2b)–to

reveal differing trends in the leaf gas-regulation strategy of Qinghai spruce (Saurer et al., 2004). A statistical correction method (McCarroll and Loader, 2004) was used to take into account the discrimination effect from rising CO_2 (i.e., the Suess effect) caused by increases in anthropogenic emissions, and thus generate the corrected $\delta^{13}C$ series ($\delta^{13}C_{cor}$, Fig. S5).

To distinguish the independent influence of climate and atmospheric CO_2 upon iWUE, we estimated the percent changes in iWUE driven by CO_2 (iWUE-c_a) and by climate (iWUE-climate), respectively, since the 1840s (Figs. 2c and S8c) based on the method of Voelker et al. (2016). These two components of iWUE were obtained to identify whether climate or CO_2 (or both) indirectly affected tree growth via ecophysiological responses driven by an improved iWUE (Voelker et al., 2016).

2.5. Data analyses

Using segmented regression models designed in the '*segmented*' package for R (Muggeo, 2017), we determined the piecewise linear dynamics in tree growth for 1840–2019. We considered one or more breakpoint years when the most significant directional (linear regression) shifts in BAI chronology occurred (Table S1). By combining the critical years emphasized by segmented models of BAI and the abrupt changepoints in climate trends, we chose five sub-periods for further analyses: 1840–1929, 1930–1964, 1965–1984, 1985–2002, and 2003–2019. Tree growth rates during these sub-periods are shown in Table S2. Linear regressions were fitted to determine whether significant temporal trends in tree-ring isotope proxies existed during each sub-period (Table S2).

The climatic responses of BAI and stable isotope chronologies were assessed using Pearson's correlation coefficient (Figs. S6 and S7). The temporal windows used for analysis were monthly (from the previous June through the current September) and multi-monthly. We also applied the first-order difference (fod) calculation to the correlations, to obtain linkages on high-frequency variation.

Two linear mixed-effects models (LMMs) were built to characterize the BAI patterns as a function of environmental and ecophysiological parameters over several sub-periods (Tables S4 and S5), using the '*lme4*' package for R (Bates et al., 2015). Fixed effects of the first model included c_a, iWUE, and $\delta^{15}N$, while the second model tested the effects of $\delta^{15}N$ and the two components of iWUE driven by CO_2 (iWUE-c_a) and climate (iWUE-climate) separately. We used the second LMM to identify whether CO_2 fertilization could affect BAI through an improved iWUE. Each predictor variable was standardized, by calculating its Z-scores, before any model fitting, to enable direct comparisons. Tree ontogenetic stage was introduced as a random effect considering five age classes: young, < 20 years; middle-aged, 21–120 years; near-mature, 121–140 years; mature, 141–180 years; and over-mature, > 180 years (Wang, Che et al., 2000). Marginal and conditional R^2 values were calculated, using the '*MuMIn*' package for R (Bartoń, 2022), to express the proportion of variance explained by fixed factors and fixed-plus-random factors, respectively. We also ran both LMMs for tree-ring $\delta^{15}N$ for each of the five sub-periods from the beginning of climatic records, to check for the potential effects of variation in environmental factors (Table S3).

The individual contribution of each fixed factor to BAI variability (Fig. 4) was

quantified using the '*glmm.hp*' package for R (Lai and Nimon, 2022). This method uses hierarchical partitioning to estimate the importance of each explanatory variable under an unordered assessment of the total variance for each LMM of BAI (Lai and Nimon, 2022). The significance level was set at $p < 0.05$. All statistical analyses were implemented in R v4.1.3 (R Core Team, 2022).

3. Results

3.1. Climate trends

From 1958 to 2019, the trends in observed temperature, total precipitation, and VPD were significantly ($p < 0.001$) positive (0.039 °C year^{-1}; 1.312 mm year^{-1}; 0.002 kPa year^{-1}), but RH decreased over time (−0.054 % year^{-1}, $p < 0.001$) (Fig. S1c). Using the CRU data spanning a longer period (Fig. S2), similar shifts in temperature and VPD were detected while precipitation increased (0.539 mm year^{-1}) from 1935 to 2019. Temperature declined before 1968 (−0.028 °C year^{-1}) but later increased (0.016 °C year^{-1}). Similarly, VPD increased after 1964. The climate data obtained from meteorological stations and CRU TS 4.04 were strongly correlated ($r > 0.665$, $p < 0.01$) and featured similar variability in temperature, precipitation, and VPD (Fig. S3).

3.2. Growth dynamics

Spruce BAI changed little (−0.007 cm^2 year^{-1}) during from 1840 to 1929 (Fig. 1a and Table S2). However, trees began to undergo sustained increases in their growth rates during the 1930s (0.140 cm^2 year^{-1}, $p < 0.001$), followed by smaller increases in 1965−1985 (0.111 cm^2 year^{-1}). The rate of tree growth then declined around 1985 and this negative trend persisted until the early 2000s (−0.396 cm^2 year^{-1}, $p < 0.001$). After

that, tree growth accelerated significantly (0.736 cm^2 $year^{-1}$, $p < 0.001$), reaching its highest rate since 1840.

This dynamic growth pattern over the last 180 years was in agreement with the synchronous changes in BAI across all 22 sampled trees (Fig. 1a). Since trees had narrow ranges of DBH (30–60 cm, mean 44.0 ± 6.9 cm; Fig. 1b) and age (160−230 years, mean: 179 ± 17 years; Fig. 1c). Therefore, age-related changes in growth rates cannot explain the recent growth trends of Qinghai spruce in the study region.

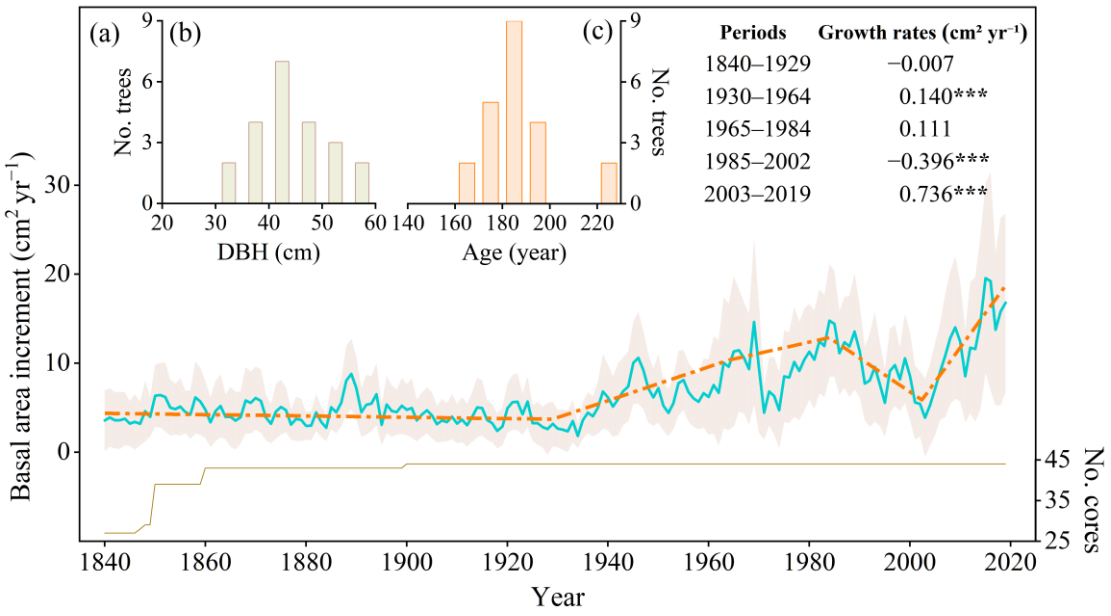

Fig. 1. Tree growth pattern of mature Qinghai spruce. (a) Variation in tree radial growth expressed as basal area increment (BAI) from 1840 through 2019. The shaded area represents the standard deviation of all samples. The right y–axis shows the sample number of tree cores. Annual growth rates of different sub-periods are the slope values of linear regressions, these are indicated by conjoined dashed lines. Significance levels: *, $p < 0.05$; **, $p < 0.01$; ***, $p < 0.001$. Detailed regression estimates are shown in Tables S1 and S2. Histograms show the distribution of sampled trees grouped as a function of (b) stem diameter at breast height (DBH), and (c) age.

3.3. Variability of tree-ring iWUE and $\delta^{15}N$

The $\delta^{13}C_{cor}$ series had a positive trend from 1985 to 2002 (0.036 ‰ $year^{-1}$, $p < 0.05$) (Fig. S8a and Table S2). The trend for c_i/c_a turned negative from 1985 to 2002 (−0.0016, $p < 0.05$; Fig. S8b). From 1840 to 1929, tree-ring iWUE increased (0.086 µmol mol^{-1},

$p < 0.001$), then it remained stable from 1930 to 1984, after which it rose from 1985 to 2019, increasing the most in 1985–2002 (0.809 μmol mol^{-1}, $p < 0.001$, Fig. 2a). Variation in iWUE closely followed the constant c_i/c_a scenario (Fig. 2b).

Before 1929, tree-ring $\delta^{15}N$ remained stable, then it increased from 1930 to 1964 (0.122 ‰ $year^{-1}$, $p < 0.001$), after which it decreased at a mean rate of −0.228 ‰ $year^{-1}$ from 1965 to 2019, especially in 1985–2002 (−0.315‰ $year^{-1}$, $p < 0.001$) (Fig. 3a and Table S2). The 21-year running correlations revealed an overall positive relationship ($p < 0.05$) between tree-ring $\delta^{15}N$ and growth during the past century (Fig. 3b). Tree-ring $\delta^{15}N$ and BAI covaried from 1920–2000, whether based on raw data ($r = 0.353$, $p < 0.001$) or high-frequency data ($r = 0.501$, $p < 0.01$) (Fig. 3c, d). The role of $\delta^{15}N$ in modulating tree growth is best illustrated through the LMMs (see section 3.6). Changes in tree-ring $\delta^{15}N$ were consistent with those of wood C/N ($r = 0.588$, $p < 0.001$) in 1840–2019 (Fig. S9a). Wood C/N declined in 1840–1929 (slope = −1.366, $p < 0.001$), rebounded significantly in 1930–1964 (slope = 4.625, $p < 0.05$), and then fell at a mean rate of −14.482 $year^{-1}$ between 1965 and 2019 (Fig. S9a and Table S2).

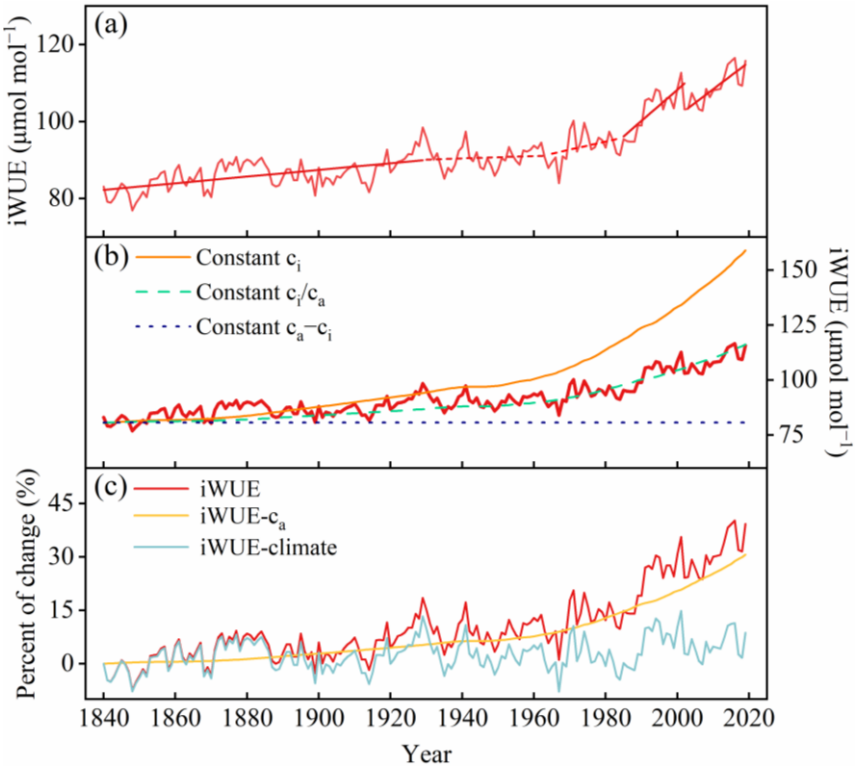

Fig. 2. (a) Chronologies of intrinsic water-use efficiency (iWUE); thick solid lines represent significant ($p < 0.05$) increasing or decreasing trends, while dashed lines indicate non-significant trends (regression estimates for five different sub-periods can be found in Table S2). (b) Tree-ring iWUE variation alongside the modeled baselines of three scenarios for the theoretical regulation of plant gas exchange in response to rising c_a. (c) Relative change in iWUE, iWUE-c_a, and iWUE-climate over time.

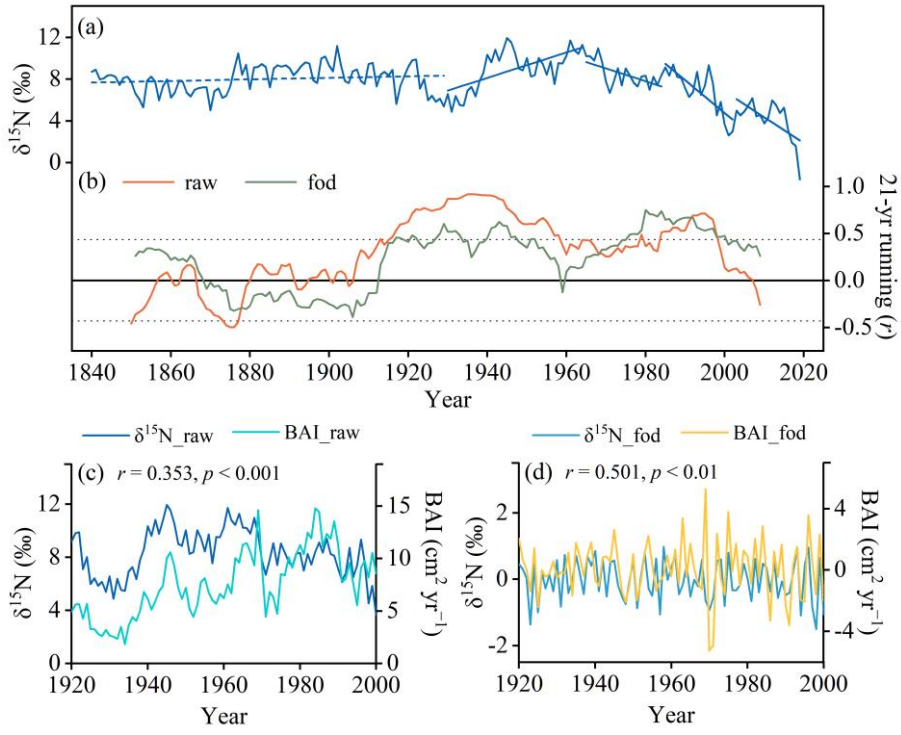

Fig. 3. (a) Tree-ring nitrogen isotope ratio ($\delta^{15}N$) in mature Qinghai spruce as a function of time.

Linear trends are depicted for five different sub-periods. Significant ($p < 0.05$) trends (increasing or decreasing) are shown as thick solid lines; non-significant trends appear as dashed lines (regression estimates can be found in Table S2). (b) The 21-year running correlation coefficients of tree growth (BAI) and $\delta^{15}N$ calculated considering the raw data or first-order differences (fod). The dotted lines in panel (b) indicate thresholds for $p = 0.05$. Comparison of tree-ring $\delta^{15}N$ and BAI during the 1920–2000 period based upon (c) raw values or (d) first-order differences (fod); their corresponding correlation coefficients and *p*-values are also shown.

3.4. Contribution of multiple drivers to tree growth

The response patterns of BAI revealed a weak climatic signal (Figs. S6a, d and S7a, d). BAI was positively correlated with June–July precipitation, RH, and scPDSI, but negatively with early summer temperature and VPD. These relationships indicated some dependence of growth on moisture availability.

Changes in BAI from 1840 to 1929 were associated with increases in iWUE (Fig. 4a and Table S4), specifically in iWUE-climate (Fig. 4b and Table S5), which contributed most to the enhanced iWUE during this sub-period. From 1930 to 1964, the marked increases in $\delta^{15}N$ substantially augmented BAI, though iWUE was also a significant predictor (Table S4); the change in iWUE-climate explained little of the variance in BAI (Fig. 4b). A greater $\delta^{15}N$ was responsible for the largest change in BAI, accounting for 49.13% of its variance between 1930 and 1964 (Fig. 4a), corresponding to the synchronous variation between these two parameters (Fig. 3c). From 1965 to 1984, iWUE was marginally related to BAI (Table S4). From 1985 to 2002, however, the general increase in iWUE became the chief factor determining the reduction in tree growth, explaining 43.02% of its variance (Fig. 4a), of which the iWUE-climate component explained 28.29% of the BAI variability (Fig. 4b). Finally, from 2003 to 2019, iWUE underwent linear increases in tandem with the recent surge in BAI (Table S4) and this contributed positively (60.00%) to the BAI increases (Fig. 4a). A

significantly positive effect of iWUE-c_a on BAI was also detected (Table S5), which explained 55.76% of the BAI variance (Fig. 4b).

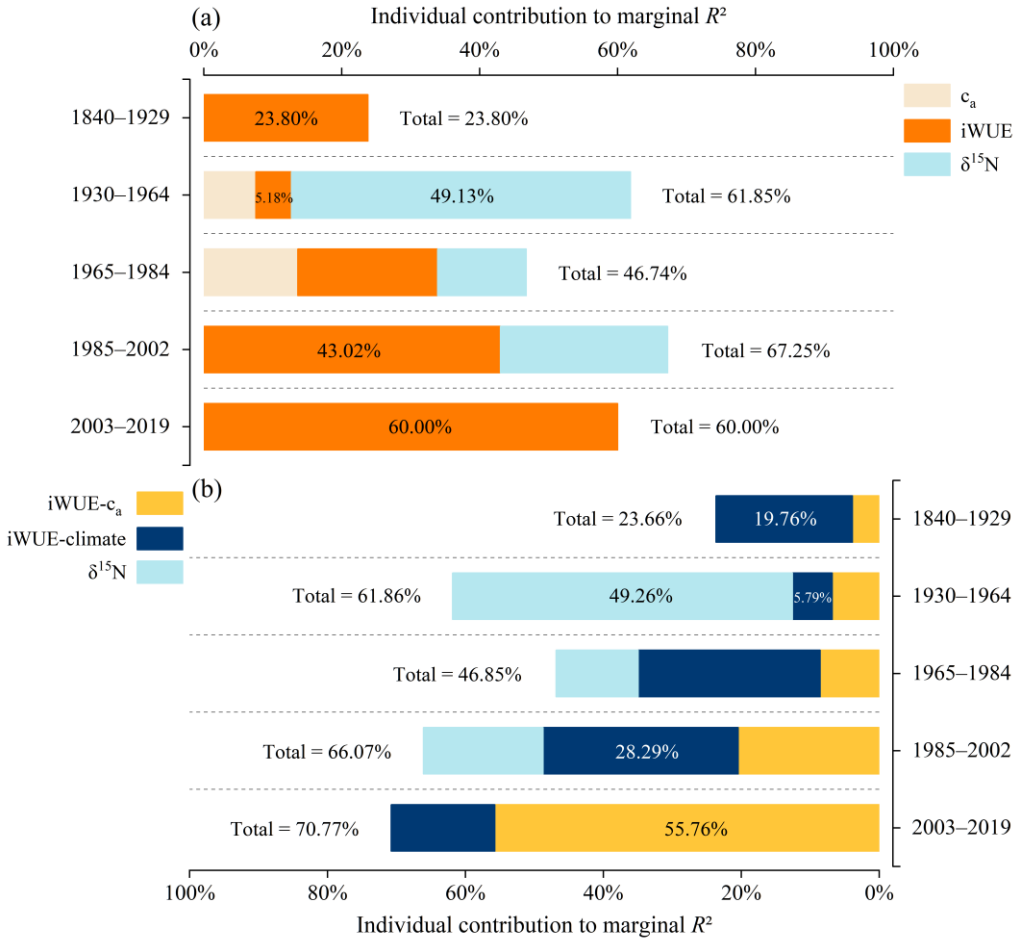

Fig. 4. Respective contribution of each fixed effect towards the total marginal R^2 based on linear mixed-effects models (LMMs) fitted to tree growth (BAI) during five different sub-periods. The results of LMMs are presented separately in Tables S4 (for Fig. 4a) and S5 (for Fig. 4b). Fixed effects of the first LMM included c_a, iWUE, and $\delta^{15}N$ (a), while the second LMM focused on $\delta^{15}N$ and the two components of iWUE (iWUE-c_a and iWUE-climate) separately driven by CO_2 and climate (b). We used the second LMM to determine whether CO_2 fertilization affects growth via an improved iWUE. Note that only significant effects ($p < 0.05$) are labeled with percentage numbers.

4. Discussion

Our study offers a novel perspective on the underlying drivers shaping growth dynamics of mature, drought-prone forest trees and their ecophysiological responses to rising CO_2, global warming, and changes in nitrogen availability. As such, this work advances our understanding of the carbon sink potential of mature trees over the long

term in semi-arid mountain ecosystems.

We identified three main growth phases of Qinghai spruce since 1930 (Fig. 5): (i) a phase characterized by a sustained increase in growth, from 1930 to 1964; (ii) a phase characterized by remarkable growth decline, from 1985 to 2002; and (iii) a phase characterized by unprecedented surges in growth rates, from 2003 to 2019. The LMMs revealed that several environmental and ecophysiological predictors, i.e., c_a, iWUE (both iWUE-c_a and iWUE-climate), as well as $\delta^{15}N$, significantly affected tree growth. However, the response of BAI to each variable differed in strength and direction during the different sub-periods.

Fig. 5. Conceptual model showing how the dynamic interplay of climatic factors, nitrogen availability, and atmospheric CO_2 influences the growth of mature Qinghai spruce over time.

4.1. Tree growth benefited from improved nitrogen availability

Increasing nitrogen availability mainly arose via changes in bioavailable nitrogen pools, which coincided with favorable climate conditions and low c_a in 1930–1964 (Table S3). The level of anthropogenic nitrogen inputs at our study site was very low, considering it belongs to remote mountain areas that are neither rapidly industrialized nor densely populated. The data evidences supporting the above argument were detailed in Wang et al. (2022). Therefore, our tree-ring $\delta^{15}N$ signatures mainly reflected internal nitrogen processes in the study stand. Climate change and rising c_a may generate long-term modifications to soil nitrogen processes and nitrogen availability (Savard and Siegwolf, 2022). On the one hand, the colder climate correlated negatively with the variation in nitrogen availability (Table S3). Climate-driven changes in soil hydrologic conditions alter key mechanisms of nitrogen cycling (Greaver et al., 2016). As reported earlier (Liang et al., 2006), there was a severe and sustained drought in the 1920s and early 1930s across northern China. Drought can inhibit nitrification and cause nitrogen to accumulate in soil, but nitrification pulses can occur in response to abundant rainfall (Wang et al., 2015). Moreover, because wetter climate conditions should increase rates of denitrification, more ^{15}N-depleted nitrogen would be lost via the gas phase (Duncan et al., 2013). These nitrogen cycling processes tend to strongly discriminate against ^{15}N, thus increasing soil and/or plant $\delta^{15}N$, ultimately resulting in higher availability of nitrogen (Elmore et al., 2016). On the other hand, tree-ring $\delta^{15}N$ increased in tandem with the rising c_a over time (Table S3). CO_2-reduction experiments and evidence from

periods of low CO_2 might provide a possible explanation for the positive effects of c_a on plant nitrogen concentrations and nitrogen mineralization in soil (Ripley et al., 2013).

In our study, BAI benefited primarily from increasing nitrogen availability (Fig. 4a and Table S4), similar to the improved nutrient availability after permafrost thawing at a high-latitude site (Silva et al., 2016). Reductions in competitive pressure triggered by growth releases might also explain, in part, the surges in growth of Qinghai spruce after the dry 1920s (Liang et al., 2006). Forest dieback and tree death caused by severe drought and/or thinning reduce plant nitrogen uptake rates and bolster the relative retention of nitrogen in soils (McLauchlan et al., 2007). Again, the greater nitrogen availability associated with growth releases caused by that drought disturbance was likely related to the early stage of forest recovery (McLauchlan et al., 2007). In addition, the significant increases in nitrogen availability and C/N in 1930–1964 (Fig. S9) were coupled with faster tree growth. This could be due to more efficient nitrogen use to enhance plant survival when soil moisture levels are sufficient (Quadri et al., 2021; Zhang et al., 2020).

4.2. Varied growth stimulation with increasing iWUE

Across the 1840–2019 period, increased iWUE was characterized by a constant c_i/c_a scenario (Fig. 2), suggesting different leaf gas-exchange strategies of Qinghai spruce in response to changes in c_a and climatic conditions (Saurer et al., 2004). During 1985–2002, iWUE rose rapidly while the $\delta^{13}C_{cor}$ decreased and c_i/c_a increased (Figs. 2a and S8); in addition, the influence of climate was slightly greater than that of CO_2 (Fig. S8c). Our results suggest that atmospheric water demand likely influences stomatal

449 conductance, as shown by the positive relationships between early summer VPD and
450 temperature with iWUE (Fig. S6b). In the Qilian Mountains, drought conditions due to
451 higher temperatures and reduced precipitation were reported for 1980–2001 (Gao et al.,
452 2018). Thus, higher demand for atmospheric water related to warming suggests the
453 avoidance of impaired hydraulic functioning at the expense of carbon uptake. Similar
454 observations can be found in other studies that found similar tree physiological
455 responses to moisture deficit despite increases in iWUE (Giguere-Croteau et al., 2019;
456 González de Andrés et al., 2021; Wang, McDowell et al., 2020).

457 In the second phase (1985–2002), increases in iWUE negatively affected tree
458 growth (Fig. 4a and Table S4) via changed climate conditions and nitrogen availability.
459 A noticeable growth decline period between 1980 and 2001 in Qinghai spruce was also
460 confirmed in the same study area (Gao et al., 2018; Wang, Chen et al., 2020). Given the
461 positive relationships between radial growth and moisture availability, drought stress is
462 likely to be the main factor responsible for the growth reductions (Figs. S6a, d and S7a,
463 d). A negative correlation between BAI and temperature under drought conditions (Figs.
464 S6d and S7d) also implies the high sensitivity of BAI to water shortage. Again, the
465 sharp increases in iWUE may partially reverse the stem growth reduction, as evinced
466 by the greater variance of BAI explained by iWUE-climate (Fig. 4b and Table S5).
467 Lower nitrogen availability at this time (i.e., second phase) may also have been a factor
468 limiting the capacity of augmented iWUE to stimulate tree growth, though this effect
469 could not be confirmed here. Altogether, these results suggest that the lack of growth
470 stimulation in spite of an increasing iWUE can be jointly explained by climate change,

particularly drought stress, stomatal density reduction, and nutrient limitation (Giguere-Croteau et al., 2019; González de Andrés et al., 2021; Wang, McDowell et al., 2020).

4.3. Recent accelerated growth was mainly driven by CO_2 fertilization

During 2003–2019, the stimulation by increasing CO_2 levels might have been responsible for the stark increase in iWUE (Fig. S8c). The trend of increasing precipitation at our study site also indicated greater availability of moisture, enabling more stomata to remain open longer (Figs. S1c and S2). These conditions would have allowed higher carbon assimilation to be the major driver of increases in iWUE, which other studies have also highlighted (Guerrieri et al., 2019; Palandrani et al., 2021; Rayback et al., 2020).

Faster radial growth in 2003–2019 was largely attributed to that period's CO_2 fertilization effect coupled with increased iWUE (Fig. 4). The positive correlation we found between BAI and iWUE or iWUE-c_a (Tables S4 and S5) provides supporting evidence that rising c_a could stimulate photosynthesis and then tree growth, consistent with other findings of enhanced photosynthesis being the major driver of increased iWUE and BAI (Guerrieri et al., 2019; Palandrani et al., 2021).

4.4. Declining nitrogen availability did not limit tree growth in recent decades

Continuous declining nitrogen availability, as indicated by tree-ring $\delta^{15}N$, occurred in 1965–2019 when the c_a was higher and the climate was warmer (Table S3). Rising temperature- and CO_2-induced changes to soil water deficits could alter both net nitrogen mineralization rates and plant nitrogen demand, especially in water-limited regions (Mason et al., 2022). On the one hand, warmer early summers led to decreased

tree-ring $\delta^{15}N$ (Table S3); however, some studies did not find this negative relationship when trying to explain changes in foliar or tree-ring $\delta^{15}N$ across ecosystems concerning climatic factors (Guerrieri et al., 2020; Tang et al., 2022). An increasing temperature may extend the plant-growing season, especially in high-altitude mountainous regions, strengthening the plant demand for nitrogen such that its supply is exceeded, thereby reducing its availability in soil (Craine et al., 2018; Elmore et al., 2016). Higher air temperatures can also induce soil water deficits that negatively influence the net mineralization rates of nitrogen (Churkina et al., 2010). Furthermore, rising temperatures generally stimulate microbial activity, shortening the residence time of organic matter in soil and increasing the supply of bioavailable nitrogen to plants (Hobbie and Högberg, 2012). On the other hand, we found that higher and increasing c_a negatively affect nitrogen availability (Table S3), consistent with previous studies (Craine et al., 2018; McLauchlan et al., 2010, 2017]. Rising CO_2 enhances the rate of photosynthesis, which increases the demand for plant-available soil nitrogen and lowers the overall nitrogen availability (Luo et al., 2004). A greater c_a may also reduce the net mineralization of nitrogen and diminish its supply in soil, and hence its uptake by plants (Billings and Ziegler, 2005). Nitrogen availability can be also reduced by increasing organic storage with rising CO_2, namely in wood biomass and recalcitrant plant litter, and via enhanced microbial immobilization (Luo et al., 2004).

The synchronous decline of $\delta^{15}N$ and C/N in 1965–2019 (Fig. S9a) may also suggest a decrease in soil nitrogen availability because of increased nitrogen sequestration in wood. One possible explanation is progressive nitrogen limitation, whereby nitrogen

availability declines as a result of increasing sequestration by organic pools, including microbial biomass, wood, and recalcitrant plant litter (Luo et al., 2004; McLauchlan et al., 2010). The decreased wood $\delta^{15}N$ might have resulted from a more closed nitrogen cycle in the ecosystem with less nitrogen deposition in remote areas, implying less ^{14}N-enriched nitrogen was lost through denitrification and/or nitrate-flushing processes (Craine et al., 2015). Consequently, nitrogen's uptake and retention by plants increased with greater demand for it, by them absorbing ^{15}N-depleted nitrogen from soils and/or relying more on the symbiotic associations with fungi that provide light nitrogen (Hobbie and Högberg, 2012). This interpretation is further supported by the declining wood C/N, driven largely by augmented tree-ring nitrogen storage (Fig. S9). Furthermore, lower C/N values are often found when plants tend to compete for more carbon gain when their growing conditions are favorable (Zhang et al., 2020).

In the last phase, 2003–2019, tree growth was not markedly constrained by declining nitrogen availability but in fact enhanced by CO_2 fertilization. This suggests that large and mature Qinghai spruce forests still retain high potential as carbon sinks. Significant positive relationships between tree-ring $\delta^{15}N$ and growth (Figs. 3c and d) were detected during the 1920–2000 period. Our results emphasize that the recent declining nitrogen availability did not reduce growth, suggesting a shift from nitrogen to CO_2 as the driving force of mature tree growth dynamics. During this period, the positive effect of increased CO_2 on tree growth may have outweighed any detrimental effects of nitrogen limitation, and also possibly benefited from greater water availability.

5. Conclusions

This study elucidated the environmental and ecophysiological drivers of radial growth patterns of mature Qinghai spruce over the last 180 years, specifically the underlying factors contributing to recent growth accelerations. Tree growth started to increase in 1930 and growth rates accelerated over the last two decades. Nitrogen availability positively affected growth with a substantial yet dynamic impact from the 1920s onwards. Recent accelerated growth was driven primarily by CO_2 fertilization, possibly due to higher photosynthesis rates. Tree growth of mature spruce was not markedly constrained by gradual nitrogen limitation as the higher CO_2 levels and increasing temperatures since 2000. Our results also emphasize the need to explicitly consider how long-term carbon-nitrogen interactions, in addition to water stress, contribute to trees' nitrogen dynamics and acquisition in mountain conifer forests. This would benefit accurate assessments of the current and future potential of the productivity and carbon storage potential of forests in temperate, seasonally dry mountainous regions in the face of ongoing environment change.

Declaration of Competing Interest

The authors declare that they have no conflict of interest.

Data availability

The monthly meteorological data used in the study was downloaded from the China Meteorological Data Service Center (http://data.cma.cn) and CRU TS 4.04 datasets (Harris et al., 2020). The estimated annual values of c_a and $\delta^{13}CO_2$ were obtained from Belmecheri and Lavergne (2020). The R code of linear mixed-effects model was obtained from the 'lme4' and 'MuMIn' packages for R (Bartoń, 2022; Bates et al., 2015). The data of tree-ring widths and stable carbon ($\delta^{13}C$) and nitrogen ($\delta^{15}N$) isotopes will be freely obtained from Liu (Liu, 2023).

Acknowledgments

This work was supported by the National Natural Science Foundation of China (grant number 41971104, 42277448, and 42330501). We would like to thank Huhu Kang (Northwest Institute of Eco-Environment and Resources, Chinese Academy of Sciences), Yu Zhang and Wensen Ge (School of Geography and Tourism, Shaanxi Normal University) for their help in tree ring sampling. Josep Peñuelas was supported by the Spanish Government grants PID2020115770RB-I, TED2021-132627 B–I00 and PID2022-140808NB-I00, funded by MCIN, AEI/10.13039/ 501100011033 European Union Next Generation EU/PRTR, the Fundación Ramón Areces grant CIVP20A6621, and the Catalan Government grant SGR 2021–1333.

References

Bartoń, K., 2022. MuMIn: Multi-model inference. R package version 1.46.0. https://CRAN.R-project.org/package=MuMIn

Bates, D., Mächler, M., Bolker, B., Walker, S., 2015. Fitting linear mixed-effects models using lme4. J. Stat. Softw. 67, 1–48. https://doi.org/10.18637/jss.v067.i01

Belmecheri, S., Lavergne, A., 2020. Compiled records of atmospheric CO_2 concentrations and stable carbon isotopes to reconstruct climate and derive plant ecophysiological indices from tree rings. Dendrochronologia 63, 125748. https://doi.org/10.1016/j.dendro.2020.125748

Billings, S.A., Ziegler, S.E., 2005. Linking microbial activity and soil organic matter transformations in forest soils under elevated CO_2. Glob. Chang. Biol. 11, 203–212. https://doi.org/10.1111/j.1365-2486.2005.00909.x

Biondi, F., Qeadan, F., 2008. A theory-driven approach to tree-ring standardization: defining the biological trend from expected basal area increment. Tree Ring Res. 64, 81–96. https://doi.org/10.3959/2008-6.1

Bunn, A., Korpela, M., Biondi, F., Campelo, F., Mérian, P., Qeadan, F., et al., 2022. dplR: Dendrochronology Program Library in R. R package version 1.7.3. https://CRAN.R-project.org/package=dplR

Camarero, J.J., Gazol, A., Tardif, J.C., Conciatori, F., 2015. Attributing forest responses to global-change drivers: limited evidence of a CO_2-fertilization effect in Iberian pine growth. J. Biogeogr. 42, 2220–2233. https://doi.org/10.1111/jbi.12590

Churkina, G., Zaehle, S., Hughes, J., Viovy, N., Chen, Y., Jung, M., et al., 2010. Interactions between nitrogen deposition, land cover conversion, and climate change determine the contemporary carbon balance of Europe, Biogeosciences 7, 2749–2764. https://doi.org/10.5194/bg-7-2749-2010

Cienciala, E., Altman, J., Doležal, J., Kopáček, J., Štěpánek, P., Ståhl, G., 2018. Increased spruce tree growth in Central Europe since 1960s. Sci. Total. Environ. 619–620, 1637–1647. https://doi.org/10.1016/j.scitotenv.2017.10.138

Cook, E.R., 1985. A Time Series Analysis Approach to Tree Ring Standardization. The University of Arizona, Tucson.

Craine, J.M., Brookshire, E.N.J., Cramer, M.D., Hasselquist, N.J., Koba, K., Marin-Spiotta, E., et al., 2015. Ecological interpretations of nitrogen isotope ratios of terrestrial plants and soils. Plant Soil 396, 1–26. https://doi.org/10.1007/s11104-015-2542-1

Craine, J.M., Elmore, A.J., Wang, L., Aranibar, J., Bauters, M., Boeckx, P., et al., 2018. Isotopic evidence for oligotrophication of terrestrial ecosystems. Nat. Ecol. Evol. 2, 1735–1744. https://doi.org/10.1038/s41559-018-0694-0

Duncan, J.M., Groffman, P.M., Band, L.E., 2013. Towards closing the watershed nitrogen budget: Spatial and temporal scaling of denitrification. J. Geophys. Res. Biogeosci. 118, 1105–1119. http://dx.doi.org/10.1002/jgrg.20090

Duncan, R., 1989. An evaluation of errors in tree age estimates based on increment cores in kahikatea (*Dacrycarpus dacrydioides*). New Zealand Nat. Sci. 16, 31–37.

Ehleringer, J.R., Hall, A.E., Farquhar, G.D., 1993. Stable isotopes and plant carbon-water relations. Academic Press, San Diego.

Elmore, A.J., Nelson, D.M., Craine, J.M., 2016. Earlier springs are causing reduced nitrogen

availability in North American eastern deciduous forests. Nat. Plants 2, 16133. https://doi.org/10.1038/nplants.2016.133

Farquhar, G.D., O'Leary, M.H., Berry, J.A., 1982. On the relationship between carbon isotope discrimination and the intercellular carbon dioxide concentration in leaves. Aust. J. Plant Physiol. 9, 121–137. https://doi.org/10.1071/PP9820121

Fernández-Martínez, M., Vicca, S., Janssens, I.A., Ciais, P., Obersteiner, M., Bartrons, M., et al., 2017. Atmospheric deposition, CO_2, and change in the land carbon sink. Sci. Rep. 7, 9632. https://doi.org/10.1038/s41598-017-08755-8

Friedlingstein, P., Jones, M.W., O'Sullivan, M., Andrew, R.M., Bakker, D.C.E., Hauck, J., et al., 2022. Global carbon budget 2021. Earth Syst. Sci. Data 14, 1917–2005. https://doi.org/10.5194/essd-14-1917-2022

Gao, L., Gou, X., Deng, Y., Wang, Z., Gu, F., Wang, F., 2018. Increased growth of Qinghai spruce in northwestern China during the recent warming hiatus. Agric. For. Meteorol. 260–261, 9–16. https://doi.org/10.1016/j.agrformet.2018.05.025

Gerhart, L.M., McLauchlan, K.K., 2014. Reconstructing terrestrial nutrient cycling using stable nitrogen isotopes in wood. Biogeochemistry 120, 1–21. https://doi.org/10.1007/s10533-014-9988-8

Giguere-Croteau, C., Boucher, E., Bergeron, Y., Girardin, M.P., Drobyshev, I., Silva, L.C.R., et al., 2019. North America's oldest boreal trees are more efficient water users due to increased [CO_2], but do not grow faster. Proc. Natl. Acad. Sci. USA 116, 2749–2754. https://doi.org/10.1073/pnas.1816686116

González de Andrés, E., Suárez, M.L., Querejeta, J.I., Camarero, J.J., 2021. Chronically low nutrient concentrations in tree rings are linked to greater tree vulnerability to drought in *Nothofagus dombeyi*. Forests 12, 1180. https://doi.org/10.3390/f12091180

Grassi, G., House, J., Dentener, F., Federici, S., den Elzen, M., Penman, J., 2017. The key role of forests in meeting climate targets requires science for credible mitigation. Nat. Clim. Change 7, 220–226. https://doi.org/10.1038/nclimate3227

Greaver, T.L., Clark, C.M., Compton, J.E., Vallano, D., Talhelm, A.F., Weaver, C.P., et al., 2016. Key ecological responses to nitrogen are altered by climate change. Nat. Clim. Change 6, 836–843. https://doi.org/10.1038/nclimate3088

Guerrieri, R., Belmecheri, S., Ollinger, S.V., Asbjornsen, H., Jennings, K., Xiao, J., et al., 2019. Disentangling the role of photosynthesis and stomatal conductance on rising forest water-use efficiency. Proc. Natl. Acad. Sci. USA 116, 16909–16914. https://doi.org/10.1073/pnas.1905912116

Guerrieri, R., Vanguelova, E., Pitman, R., Benham, S., Perks, M., Morison, J.I.L., et al., 2020. Climate and atmospheric deposition effects on forest water use efficiency and nitrogen availability across Britain. Sci. Rep. 10, 12418. https://doi.org/10.1038/s41598-020-67562-w

Harris, I., Osborn, T.J., Jones, P., Lister, D., 2020. Version 4 of the CRU TS monthly high-resolution gridded multivariate climate dataset. Sci. Data 7, 109. https://doi.org/10.1038/s41597-020-0453-3

Hember, R.A., Kurz, W.A., Girardin, M.P., 2019. Tree ring reconstructions of stemwood biomass indicate increases in the growth rate of black spruce trees across boreal forests of Canada. J. Geophys. Res. Biogeosci. 124, 2460–2480. https://doi.org/10.1029/2018JG004573

Hobbie, E.A., Högberg, P., 2012. Nitrogen isotopes link mycorrhizal fungi and plants to nitrogen

dynamics. New Phytol. 196, 367–382. https://doi.org/10.1111/j.1469-8137.2012.04300.x
Holmes, R.L., 1983. Computer-assisted quality control in tree-ring dating and measurement. Tree Ring Res. 43, 69–78.
Jiang, M., Medlyn, B.E., Drake, J.E., Duursma, R.A., Anderson, I.C., Barton, C.V.M., et al., 2020. The fate of carbon in a mature forest under carbon dioxide enrichment. Nature 580, 227–231. https://doi.org/10.1038/s41586-020-2128-9
Jiao, W., Wang, L., Smith, W.K., Chang, Q., Wang, H., D'Odorico, P., 2021. Observed increasing water constraint on vegetation growth over the last three decades. Nat. Commun. 12, 3777. https://doi.org/10.1038/s41467-021-24016-9
Kou, D., Yang, G., Li, F., Feng, X., Zhang, D., Mao, C., et al., 2020. Progressive nitrogen limitation across the Tibetan alpine permafrost region. Nat. Commun. 11, 3331. https://doi.org/10.1038/s41467-020-17169-6
Lai, J., Nimon, K., 2022. glmm.hp: Hierarchical partitioning of marginal R^2 for generalized mixed-effect models. R package version 0.0-2. https://CRAN.R-project.org/package=glmm.hp
Li, D., Liu, D., 2000. Climate in Gansu. China Meteorological Press, Beijing. (In Chinese)
Liang, E., Leuschner, C., Dulamsuren, C., Wagner, B., Hauck, M., 2016. Global warming-related tree growth decline and mortality on the north-eastern Tibetan plateau. Clim. Change 134, 163–176. https://doi.org/10.1007/s10584-015-1531-y
Liang, E., Liu, X., Yuan, Y., Qin, N., Fang, X., Huang, L., et al., 2006. The 1920s drought recorded by tree rings and historical documents in the semi-arid and arid areas of Northern China. Clim. Change 79, 403–432. https://doi.org/10.1007/s10584-006-9082-x
[dataset] Liu, X., 2023. The data of tree-ring widths and stable carbon and nitrogen isotopes of mature Qinghai spruce in the central Qilian Mountains. figshare. https://figshare.com/s/f8de58c215a63d8b09d9
Luo, Y., Su, B., Currie, W.S., Dukes, J.S., Finzi, A., Hartwig, U., et al., 2004. Progressive nitrogen limitation of ecosystem responses atmospheric carbon dioxide. BioScience 54, 731–739. https://doi.org/10.1641/0006-3568(2004)054[0731:PNLOER]2.0.CO;2
Mason, R.E., Craine, J.M., Lany, N.K., Jonard, M., Ollinger, S.V., Groffman, P.M., et al., 2022. Evidence, causes, and consequences of declining nitrogen availability in terrestrial ecosystems. Science 376, eabh3767. https://doi.org/10.1126/science.abh3767
Mathias, J.M., Thomas, R.B., 2018. Disentangling the effects of acidic air pollution, atmospheric CO_2, and climate change on recent growth of red spruce trees in the Central Appalachian Mountains. Glob. Chang. Biol. 24, 3938–3953. https://doi.org/10.1111/gcb.14273
McCarroll, D., Loader, N.J., 2004. Stable isotopes in tree rings. Quat. Sci. Rev. 23, 771–801. https://doi.org/10.1016/j.quascirev.2003.06.017
McLauchlan, K.K., Craine, J.M., Oswald, W.W., Leavitt, P.R., Likens, G.E., 2007. Changes in nitrogen cycling during the past century in a northern hardwood forest. Proc. Natl. Acad. Sci. USA 104, 7466–7470. https://doi.org/10.1073/pnas.0701779104
McLauchlan, K.K., Ferguson, C.J., Wilson, I.E., Ocheltree, T.W., Craine, J.M., 2010. Thirteen decades of foliar isotopes indicate declining nitrogen availability in central North American grasslands. New Phytol. 187, 1135–1145. https://doi.org/10.1111/j.1469-8137.2010.03322.x
McLauchlan, K.K., Gerhart, L.M., Battles, J.J., Craine, J.M., Elmore, A.J., Higuera, P.E., et al., 2017. Centennial-scale reductions in nitrogen availability in temperate forests of the United States. Sci. Rep. 7, 7856. https://doi.org/10.1038/s41598-017-08170-z

Muggeo, V.M.R., 2017. Interval estimation for the breakpoint in segmented regression: a smoothed score-based approach. Aust. N. Z. J. Stat. 59, 311–322. https://doi.org/10.1111/anzs.12200

Norby, R.J., Warren, J.M., Iversen, C.M., Medlyn, B.E., McMurtrie, R.E., 2010. CO_2 enhancement of forest productivity constrained by limited nitrogen availability. Proc. Natl. Acad. Sci. USA 107, 19368–19373. https://doi.org/10.1073/pnas.1006463107

O'Leary, M.H., 1981. Carbon isotope fractionation in plants. Phytochemistry 20, 553–567. https://doi.org/10.1016/0031-9422(81)85134-5

Palandrani, C., Motta, R., Cherubini, P., Curović, M., Dukić, V., Tonon, G., et al., 2021. Role of photosynthesis and stomatal conductance on the long-term rising of intrinsic water use efficiency in dominant trees in three old-growth forests in Bosnia-Herzegovina and Montenegro. iForest 14, 53–60. https://doi.org/10.3832/ifor3414-013

Peñuelas, J., Fernández-Martínez, M., Vallicrosa, H., Maspons, J., Zuccarini, P., Carnicer, J., et al., 2020. Increasing atmospheric CO_2 concentrations correlate with declining nutritional status of European forests. Commun. Biol. 3, 125. https://doi.org/10.1038/s42003-020-0839-y

Peters, R.L., Groenendijk, P., Vlam, M., Zuidema, P.A., 2015. Detecting long-term growth trends using tree rings: A critical evaluation of methods. Glob. Chang. Biol. 21, 2040–2054. https://doi.org/10.1111/gcb.12826

Quadri, P., Silva, L.C.R., Zavaleta, E.S., 2021. Climate-induced reversal of tree growth patterns at a tropical treeline. Sci. Adv. 7, eabb7572. https://doi.org/10.1126/sciadv.abb7572

R Core Team, 2022. R: A language and environment for statistical computing. Vienna: R Foundation for Statistical Computing. https://www.R-project.org/

Rayback, S.A., Belmecheri, S., Gagen, M.H., Lini, A., Gregory, R., Jenkins, C., 2020. North American temperate conifer (*Tsuga canadensis*) reveals a complex physiological response to climatic and anthropogenic stressors. New Phytol. 228, 1781–1795. https://doi.org/10.1111/nph.16811

Ripley, B.S., Cunniff, J., Osborne, C.P., 2013. Photosynthetic acclimation and resource use by the C_3 and C_4 subspecies of *Alloteropsis semialata* in low CO_2 atmospheres. Glob. Chang. Biol. 19, 900–910. https://doi.org/10.1111/gcb.12091

Saurer, M., Siegwolf, R.T.W., Schweingruber, F.H., 2004. Carbon isotope discrimination indicates improving water-use efficiency of trees in northern Eurasia over the last 100 years. Glob. Chang. Biol. 10: 2109–2120. https://doi.org/10.1111/j.1365-2486.2004.00869.x

Savard, M.M., Siegwolf, R.T.W., 2022. Nitrogen Isotopes in Tree Rings—Challenges and Prospects, in: Siegwolf, R.T.W., Brooks, J.R., Roden, J., Saurer. M. (Eds.), Stable Isotopes in Tree Rings. Springer, Cham, pp. 361–380. https://doi.org/10.1007/978-3-030-92698-4_12

Shi, Y., Shen, Y., Li, D., Zhang, G., Ding, Y., Hu, R., et al., 2003. Discussion on the present climate change from warm-dry to warm-wet in northwest China. Quaternary Sci. 23, 152–164.

Silva, L.C.R., Sun, G., Zhu-Barker, X., Liang, Q., Wu, N., Horwath, W.R., 2016. Tree growth acceleration and expansion of alpine forests: The synergistic effect of atmospheric and edaphic change. Sci. Adv. 2, e1501302. https://doi.org/10.1126/sciadv.1501302

Stephenson, N.L., Das, A.J., Condit, R., Russo, S.E., Baker, P.J., Beckman, N.G., et al., 2014. Rate of tree carbon accumulation increases continuously with tree size. Nature 507, 90–93. https://doi.org/10.1038/nature12914

Stokes, M.A., Smiley, T.L., 1996. An Introduction to Tree-Ring Dating, second ed. University of Arizona Press, Arizona.

Tang, S., Liu, J., Gilliam, F.S., Hietz, P., Wang, Z., Lu, X., et al., 2022. Drivers of foliar ^{15}N trends in southern China over the last century. Glob. Chang. Biol. 28, 5441–5452. https://doi.org/10.1111/gcb.16285

Terrer, C., Jackson, R.B., Prentice, I.C., Keenan, T.F., Kaiser, C., Vicca, S., et al., 2019. Nitrogen and phosphorus constrain the CO_2 fertilization of global plant biomass. Nat. Clim. Chang. 9, 684–689. https://doi.org/10.1038/s41558-019-0545-2

Treydte, K.S., Frank, D.C., Saurer, M., Helle, G., Schleser, G.H., Esper, J., 2009. Impact of climate and CO_2 on a millennium-long tree-ring carbon isotope record. Geochim. Cosmochim. Acta 73, 4635–4647. https://doi.org/10.1016/j.gca.2009.05.057

Voelker, S.L., Brooks, J.R., Meinzer, F.C., Anderson, R., Bader, M.K., Battipaglia, G., et al., 2016. A dynamic leaf gas-exchange strategy is conserved in woody plants under changing ambient CO_2: evidence from carbon isotope discrimination in paleo and CO_2 enrichment studies. Glob. Chang. Biol. 22, 889–902. https://doi.org/10.1111/gcb.13102

Wang, B., Chen, T., Li, C., Xu, G., Wu, G., Liu, G., 2020. Radial growth of Qinghai spruce (*Picea crassifolia Kom.*) and its leading influencing climate factor varied along a moisture gradient. For. Ecol. Manage. 476, 118474. https://doi.org/10.1016/j.foreco.2020.118474

Wang, J., Che, K., Jiang, Z., 2000. A study on carbon balance of *Picea crassifolia* in Qilian Mountains. J. Northeast For. Univ. 15, 9–14. (In Chinese)

Wang, L., Manzoni, S., Ravi, S., Riveros-Iregui, D., Caylor, K., 2015. Dynamic interactions of ecohydrological and biogeochemical processes in water- limited systems. Ecosphere 6, 1–27. https://doi.org/10.1890/ES15-00122.1

Wang, Q., Zhai, P., Qin, D., 2020. New perspectives on 'warming-wetting' trend in Xinjiang, China. Adv. Clim. Chang. Res. 11, 252–260. https://doi.org/10.1016/j.accre.2020.09.004

Wang, W., McDowell, N.G., Liu, X., Xu, G., Wu, G., Zeng, X., et al., 2020. Contrasting growth responses of Qilian juniper (*Sabina przewalskii*) and Qinghai spruce (*Picea crassifolia*) to CO_2 fertilization despite common water-use efficiency increases at the northeastern Qinghai–Tibetan plateau. Tree Physiol. 41, 992–1003. https://doi.org/10.1093/treephys/tpaa169

Wang, Z., Liu, X., Wang, K., Zeng, X., Zhang, Y., Ge, W., et al., 2022. Tree-ring $\delta^{15}N$ of Qinghai spruce in the central Qilian Mountains of China: Is pre-treatment of wood samples necessary? J. Arid Land 14, 673–690. https://doi.org/10.1007/s40333-022-0065-1

Yan, X., Li, Q., Deng, Y., Gao, L., Gou, X., 2021. Warming-induced radial growth reduction in *Betula albosinensis*, eastern Qilian Mountains, China. Ecol. Indic. 120, 106956. https://doi.org/10.1016/j.ecolind.2020.106956

Zhang, J., He, N., Liu, C., Xu, L., Chen, Z., Li, Y., et al., 2020. Variation and evolution of C:N ratio among different organs enable plants to adapt to N-limited environments. Glob. Chang. Biol. 26, 2534–2543. https://doi.org/10.1111/gcb.14973